



# Single-layer $\text{TiO}_x$ reconstructions on $\text{SrTiO}_3$ (111): $(\sqrt{7} \times \sqrt{7})\text{R}19.1^\circ$ , $(\sqrt{13} \times \sqrt{13})\text{R}13.9^\circ$ , and related structures



Tassie K. Andersen<sup>a,\*</sup>, Shuqiu Wang<sup>b</sup>, Martin R. Castell<sup>b</sup>, Dillon D. Fong<sup>c</sup>, Laurence D. Marks<sup>a</sup>

<sup>a</sup> Department of Materials Science and Engineering, Northwestern University, Evanston, IL 60208, United States

<sup>b</sup> Department of Materials, University of Oxford, Parks Road, Oxford OX1 3PH, UK

<sup>c</sup> Materials Science Division, Argonne National Laboratory, Argonne, IL 60439, United States

## ARTICLE INFO

### Keywords:

DFT  
Polar oxide surfaces  
Surface structure  
Oxide surfaces  
Surface defects  
Strontium titanate

## ABSTRACT

The atomic structures of two reconstructions,  $(\sqrt{7} \times \sqrt{7})\text{R}19.1^\circ$  and  $(\sqrt{13} \times \sqrt{13})\text{R}13.9^\circ$ , on the  $\text{SrTiO}_3$  (111) surface were determined using a combination of density functional theory and scanning tunneling microscopy data and APW + lo density functional theory minimizations and simulations. These reconstructions belong to the same structural family made up of an interconnected, single layer of edge-sharing  $\text{TiO}_6$  and  $\text{TiO}_5[\ ]$  octahedra. This family of reconstructions between 0.5 and 1.5 excess  $\text{TiO}_2$ , representing the lowest-reported  $\text{TiO}_2$  coverages for reconstructions on this surface. This family is found to include the previously-solved  $(2 \times 2)$  reconstruction. They all follow a simple rule for surface composition, which serves as a tool for better understanding and predicting the structure of other reconstructions of arbitrary surface unit cell size on  $\text{SrTiO}_3$  (111). This reconstruction family and the calculations of surface energies for different hypothesis structures also shed light on the structure of Schottky defects observed on these reconstructed  $\text{SrTiO}_3$  (111) surfaces.

## 1. Introduction

The surface of  $\text{SrTiO}_3$  is of great interest for catalysis [1,2], as a substrate for oxide thin film growth [3,4], and for applications in oxide electronics [5–10]. As an archetypal perovskite material,  $\text{SrTiO}_3$  represents a structural ideal; it is cubic and lacks both octahedral rotations and rhombohedral distortions at room temperature. However, its relative simplicity belies the complexity hinted at by the multitude of surface structures reported on this material.

Even for the most straightforward, commonly-utilized (100) termination of  $\text{SrTiO}_3$ , a large number of reconstructions have been reported [11–32], some of which remain unsolved. Many of the solved structures have a  $\text{TiO}_2$  double layer with units of octahedral  $\text{TiO}_6$  and  $\text{TiO}_5[\ ]$  (where  $\ ]$  is an oxygen vacancy site) [29,30,33–35]. The field is no less crowded for the (110) termination of  $\text{SrTiO}_3$  [36–41], where reconstructions including the  $(n \times 1)$  series [40,41] are made up of rings of tetrahedral  $\text{TiO}_4$  units while the  $(2 \times n)$  nanostructures [42] are made up of  $\text{TiO}_5[\ ]$  and  $\text{TiO}_6$  units in an interconnected matrix yielding differently sized, surface unit cells lacking overall formal charge.

By comparison, the  $\text{SrTiO}_3$  (111) surface is both less exhaustively studied and more complex. Bulk  $\text{SrTiO}_3$  (111) can be thought of as a stacking of alternating layers of  $(\text{SrO}_3)^{4-}$  and  $(\text{Ti})^{4+}$ . Reconstructions reported on this surface have been observed to depend heavily on

substrate preparation conditions and include a  $(1 \times 1)$  [43–45],  $(9/5 \times 9/5)$  [11,46,47], two  $(2 \times 2)$  [48], a  $(\sqrt{7} \times \sqrt{7})\text{R}19.1^\circ$  [49],  $(3 \times 3)$  [11,46,47],  $(\sqrt{13} \times \sqrt{13})\text{R}13.9^\circ$  [49],  $(4 \times 4)$  [11,46,47],  $(5 \times 5)$  [47], and  $(6 \times 6)$  [11,46,47]. Of these, only the structures of the two  $(2 \times 2)$ , the  $(3 \times 3)$ , and  $(4 \times 4)$  have been determined [48]. These reconstructions were found to have structures made up of elements from both the (100) and (110) surfaces. All are terminated with double  $\text{TiO}_x$  layers. The underlying layer is composed of octahedral  $\text{TiO}_6$  and  $\text{TiO}_5[\ ]$ , like the (100) surface, while the  $\text{TiO}_x$  layer closest to vacuum is formed by interconnected  $\text{TiO}_4$  tetrahedra, like the (110) surfaces.

Here, we solve the structures of the  $(\sqrt{7} \times \sqrt{7})\text{R}19.1^\circ$  (RT7) and  $(\sqrt{13} \times \sqrt{13})\text{R}13.9^\circ$  (RT13) reconstructions on  $\text{SrTiO}_3$  (111) using a combination of scanning tunneling microscopy (STM) and density functional theory (DFT) modeling. These structures are composed of octahedral  $\text{TiO}_6$  and  $\text{TiO}_5[\ ]$  units like those found on the (100) surface, consistent with elements of already-identified  $\text{SrTiO}_3$  (111) reconstructions. When considered together, these structures belong to a family of  $\text{SrTiO}_3$  (111) reconstructions that can be generated by examining tilings of  $\text{TiO}_5[\ ]$  and  $\text{TiO}_6$  of increasing size.

## 2. Experimental

Single crystals of 0.5 wt% Nb-doped  $\text{SrTiO}_3$  (111) with epi-polished

\* Corresponding author.

E-mail address: [tassieandersen2013@u.northwestern.edu](mailto:tassieandersen2013@u.northwestern.edu) (T.K. Andersen).

surfaces were supplied by PI-KEM, U.K. Surface preparation was performed in a JEOL JSTM4500xt ultrahigh vacuum (UHV) chamber. Samples were introduced without any pre-treatment into the chambers and annealed in UHV (chamber base pressure of  $10^{-8}$  Pa) at 850 °C for 30 min. STM images at constant current were taken at room temperature using an etched tungsten tip. A detailed description of the sample preparation and STM imaging conditions can be found in ref. [49].

All DFT calculations were performed using an all-electron augmented plane wave + local orbital WIEN2k code [50]. The PBEsol [51] generalized gradient approximation and the revTPSS method [52] were employed, with an on-site exact exchange fraction of 0.5 for the Ti-d orbital electrons, similar to previous work [35]. Atomic muffin-tin radii were set to 1.55, 1.71, and 2.21 Bohrs for O, Ti and Sr respectively, with an  $r^*k_{max}$  of 6.20. For all calculations a Brillouin-zone reciprocal space sampling equivalent to a  $4 \times 4$  in-plane mesh for a (111)  $1 \times 1$  cell. Lattice parameters for the in-plane directions of the surface unit cell were set to those of the relevant DFT optimized bulk unit cell. To avoid errors a  $1 \times 1 \times 10$  supercell with at least 1.6 nm of vacuum was employed when constructing slab calculations. Atomic positions and electron density were converged simultaneously using a quasi-Newton algorithm [53] with surface cell convergence better than 0.01 eV/ $1 \times 1$ . Surface energy per ( $1 \times 1$ ) surface unit cell was calculated as  $E_{surf} = (E_{slab} - E_{STO}N_{STO} - E_{TiO_2}N_{TiO_2}) / (2 * N_1 \times 1)$ , where  $E_{slab}$  is the total enthalpy of the slab,  $E_{STO}$  for a single bulk SrTiO<sub>3</sub> unit cell,  $N_{STO}$  the number of bulk SrTiO<sub>3</sub> unit cells present,  $E_{TiO_2}$  the total enthalpy of bulk rutile TiO<sub>2</sub>,  $N_{TiO_2}$  the number of excess TiO<sub>2</sub> units, and  $N_1 \times 1$  the number of surface ( $1 \times 1$ ) unit cells. Both  $N_{STO}$  and  $N_{TiO_2}$  are determined by finding the total number of atoms in the slab construction (complete with reconstructed surface) used and determining the values of  $n$  and  $m$  for  $nSrTiO_3 \cdot mTiO_2$ . When surface energy is plotted against TiO<sub>2</sub>-excess, as in the convex hull construction, this quantity is found by normalizing to surface area such that  $TiO_{2excess} = (N_{TiO_2}) / (2 * N_1 \times 1)$ . This method resulted in an error of approximately 0.05 eV/ $1 \times 1$  surface cell.

Low energy structures from DFT were checked using STM simulations based on a modified Tersoff–Hamann approximation [54]. Additional details regarding this simulation method can be found in ref. [55] and in the Supplemental Material (Suppl. Fig. 1).

### 3. Results

An iterative method was used to find solutions for the RT7 and RT13 structures. Experimental STM, from which unit cell size, symmetry, and prominent electron density features were obtained, informed the development of structure hypotheses. Candidate structures were relaxed and their surface energies calculated using DFT. Structures were refined if necessary by comparison of the simulated STM images with the experimental data.

Imaging of the samples by STM with RT7 and RT13 reconstructions shows terraces and jagged step edges that do not follow a preferential crystallographic direction. Much of the surface is covered by ordered RT7 or RT13 domains, although significant disorder is present between the domains. Fig. 1 shows an STM image of a typical sample where both RT7 and RT13 domains are present. Additional STM of these reconstructions on different samples are provided in the Supplemental Material (Suppl. Fig. 2). Two rotational domains are observed when comparing the two RT7 areas; this feature is also present in other samples for the RT13 [49]. The unit cells of the two reconstructions as well as their rotational domains are shown with respect to the bulk SrTiO<sub>3</sub> (111) surface in Fig. 2. In Fig. 2 the rotational domains of the RT7 reconstruction are indicated by Greek letters  $\alpha$  and  $\beta$ . The STM image of the RT7 structure resembles a hexagonal-close packed arrangement of bright spots on a dark background, while the RT13 structure shows the opposite contrast and is better described as a bright honeycomb-like structure. Unit cell averaging is performed over repeated defect free unit cells of the RT7 and RT13 reconstruction using

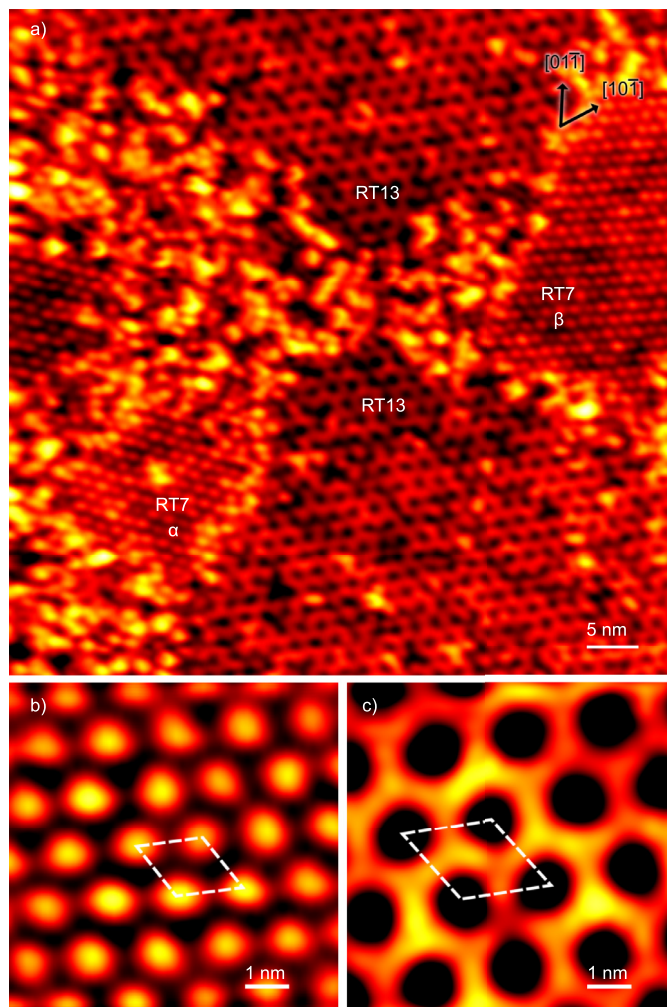
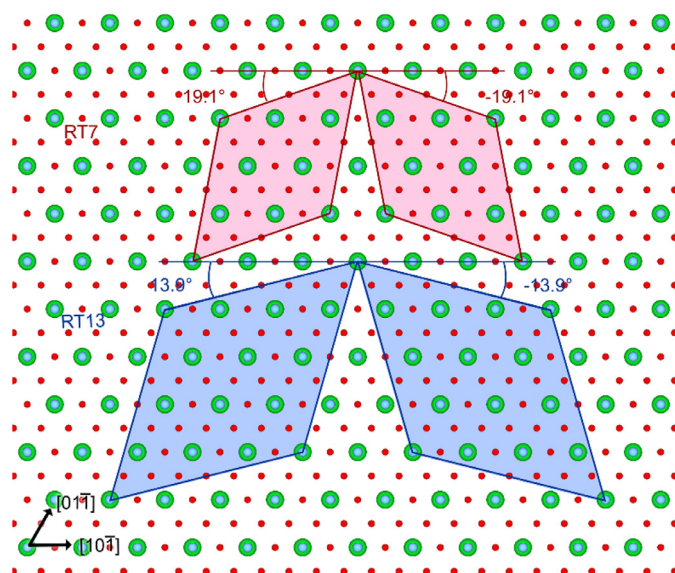


Fig. 1. (a) STM image (+2.9 V sample bias, 0.3 nA tunneling current) showing RT7 and RT13 domains. Greek letters  $\alpha$  and  $\beta$  indicate the two rotational domains of RT7. (b) Unit cell averaged STM images of the RT7 reconstruction (+2.1 V bias, 0.1 nA current) and (c) the RT13 reconstruction (+3.6 V bias, 0.1 nA current), dashed parallelograms outline unit cells of reconstructions.

the process described by Jones et al. [56]. The p3 symmetry of both reconstructions can then be identified in Fig. 1 (b, c) where the unit cells are highlighted by the white, dashed outlines.

Surface structures for SrTiO<sub>3</sub> (111) must have no overall formal charge, must be stoichiometric (i.e. with no partial occupancy of sites), and additionally are TiO<sub>2</sub>-rich based on experimental data [49]. This leads to all of the reconstructions discussed having an overall formula described by  $nSrTiO_3 \cdot mTiO_2$  where  $n$  and  $m$  are integer values. These constraints, paired with the observations from STM, lead to a limited number of possible structures following rules to be discussed in subsequent sections. Surface energies calculated from DFT for RT7 and RT13 solutions are plotted in Fig. 3. Energies from theoretical structures representing low and high TiO<sub>2</sub>-excess, chosen since they were found to be the lowest-energy possibilities among many hypothetical structures [48], are also plotted, forming endpoints. The endmember structure referred to as “Low” in Fig. 3 is composed of a single-layer, zig-zagging linear arrangement of TiO<sub>5</sub>[ ] units (this can be seen as a linear arrangement of TiO<sub>5</sub>[ ] and TiO<sub>4</sub> units as described in ref. [48] if only short Ti–O bonds between 1.8 and 2.3 Å are considered). A high-coverage structure, referred to as “High” in Fig. 3, is made up of a two-layer structure. The first layer consists of TiO<sub>6</sub> units at atomic sites which are an extension of the bulk layers below, the second layer is made of interconnected rings of TiO<sub>5</sub>[ ] units (this outer layer can be



**Fig. 2.** Unit cells of two rotational domains of RT7 (pink) and RT13 (blue) compared to the underlying in-plane bulk unit cell. Atoms of Sr (green), Ti (blue), and O (red) are shown. (For interpretation of the references to colour in this figure legend, the reader is referred to the web version of this article.)

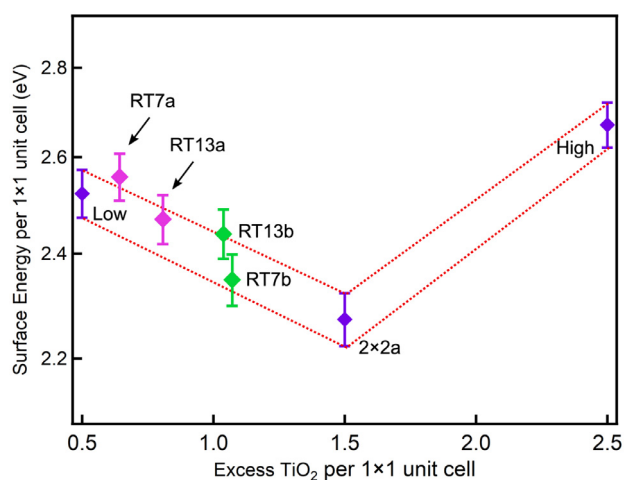


**Fig. 3.** Surface energies in eV/(1 × 1) surface unit cell plotted versus excess TiO<sub>2</sub> per (1 × 1). Results are from the revTPSS calculation, and the dotted lines show results from the convex hull construction.

seen as TiO<sub>5</sub>[ ] and TiO<sub>4</sub> units as described in ref. [48] if only short Ti–O bonds between 1.8 and 2.3 Å are considered). Together with the experimentally solved (2 × 2)<sub>a</sub> reconstruction, they form a convex hull construction. In this work these two structures will be referred to as “High” and “Low”, with the third structure plotted in the convex hull in Fig. 3 referred to as “2 × 2<sub>a</sub>”. Please note that in ref. [48] these are referred to by the terms “High”, and “Small” (ref. [48] supplement), “Low”, “L4” (ref. [48] supplement), and “2 × 2<sub>a</sub>”, “O2 × 2” (ref. [48] supplement). If the calculated surface energy for a given structure is within error of an interpolated line between these convex hull points it is considered a stable structural possibility. In Fig. 3, the lowest-energy solutions that best match the experimental STM data are those marked RT7b and RT13b. The other solutions plotted, RT7a and RT13a, are additional low-energy structure solutions. Given the accuracy of the DFT functionals, the convex hull and proposed solutions are consistent with experiment as described in previous work [48]. Both solutions for the RT7 and RT13 are lower in excess TiO<sub>2</sub> than the previously reported (2 × 2)<sub>a</sub>, making them the lowest excess TiO<sub>2</sub> reconstructions solved on

the SrTiO<sub>3</sub> (111) surface. The TiO<sub>2</sub> excess for both structures, 1.071 for RT7b and 1.038 for RT13b, is similar and consistent with the STM results showing both domains on a given sample. This reinforces the observation that identical preparation methods lead to similar surface compositions.

The simulated STM image of the RT7b structure, shown in Fig. 4 (a, b), is the closest match among the low-energy RT7 candidate structures to experimental data. These structures (RT7b and RT13b) are shown in an enlarged view and from an in-plane axis in the Supplemental Material (Suppl. Fig. 3). The bright dot features are reproduced at spacings that match experiment, and the three-fold rotation symmetry is prominent. The other low-energy structure, RT7a, is shown for comparison in Fig. 4 (c, d). The RT13 structure most consistent with experiment, RT13b, is also shown in Fig. 4 (e, f), and the features of its simulated STM image recreate the bright honeycomb-like pattern faithfully, while the other low-energy structure, RT13a, is shown in Fig. 4 (g, h). In these reconstructions, the dark areas of the experimental STM image correspond to areas lacking TiO<sub>x</sub> coverage or areas where TiO<sub>x</sub> units are present in low density such that they are not connected to as many neighboring TiO<sub>x</sub> units, as the structures in Fig. 4 (b, d, f, and h) illustrate.

Both the RT7b and RT13b structures are made up of an interconnected network of two structural features. A single surface layer of octahedrally coordinated TiO<sub>6</sub> and TiO<sub>5</sub>[ ] units forms the basis of both reconstructions. Each TiO<sub>6</sub> unit shares three polyhedron edges with TiO<sub>x</sub> units in the same surface plane, while TiO<sub>5</sub>[ ] units share only two edges. The Ti–O bond lengths in the surface TiO<sub>6</sub> and TiO<sub>5</sub>[ ] are both comparable to those in the bulk. Surface Ti to subsurface O bonds are slightly longer than in the bulk (2.209 Å for TiO<sub>6</sub> and 1.994 Å for TiO<sub>5</sub>[ ] vs 1.968 Å in the bulk), which is unsurprising as the surface TiO<sub>x</sub> units are packed more closely than in the bulk, favoring outward expansion. Bond-valence sums indicate that the titanium and oxygen atoms are close to the 4+ and 2- nominal valences, respectively, as expected from a stable structure [57]. Structures refined from DFT are provided as crystallographic information files (CIF) in the Supplemental Material accompanied by a key indicating which file names correspond to which structures.

#### 4. Discussion

Analysis of these reconstructions reveals a common model for their generation, one that was in fact used to identify initial structural hypotheses. The two reconstructions treated in this work share common structural units. They consist of a single TiO<sub>x</sub> terminating layer built up on the bulk-like SrO<sub>3</sub><sup>4-</sup> (111) atomic plane. This TiO<sub>x</sub> layer is an interconnected network of octahedral TiO<sub>5</sub>[ ] and TiO<sub>6</sub> units. Overall lack of formal charge is maintained and each oxygen atom in the layer closest to vacuum is bonded to two cations. In the case of the RT7b reconstruction, avoiding formal charge is done by removal of a single strontium atom per surface reconstruction unit cell from the otherwise bulk-like SrO<sub>3</sub><sup>4-</sup> layer. This description is codified in Fig. 5, where the imposed triangular grid has intersections at the position of Sr atoms in the outermost bulk-like SrO<sub>3</sub><sup>4-</sup> layer. The spaces within the grid represent available sites for placement of TiO<sub>5</sub>[ ] and TiO<sub>6</sub> units (red and blue respectively).

One structure, a theoretical low-energy SrTiO<sub>3</sub> (111) surface not plotted in Fig. 3 but reported as “Model 8” in ref. [58], and “Other” in ref. [48] (referred to as “Other” herein) serves as a starting point for generation of the RT7b, RT13b, and other reconstructions of this single Ti-layer family. It is made up of a bulk-like SrO<sub>3</sub><sup>4-</sup> layer with every atomic site (other than those above the strontium atoms) occupied by a titanium atom such that the terminating surface is an unbroken matrix of TiO<sub>6</sub> units. If this were to be illustrated using the coded method described above, it would appear as an unbroken field of blue triangles occupying every grid space. This structure meets the criterion of being free of overall charge and can be represented by the formula

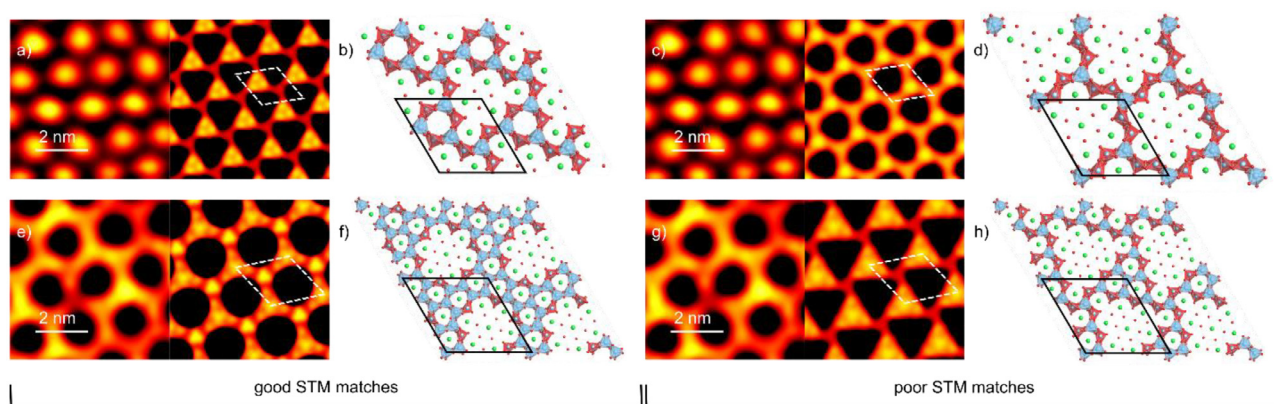


**Fig. 4.** (a) Unit cell averaged STM image (+2.1 V sample bias, 0.1 nA tunneling current) of RT7 with simulated RT7b overlaid in the middle and (b) structure diagram with  $\text{TiO}_5$  octahedra in red,  $\text{TiO}_6$  octahedra in blue, and Sr atoms in green. (c, d) Show the same information for RT7a respectively. (e) Unit cell averaged STM (+3.6 V bias, 0.1 nA current) of RT13, simulation RT13b overlaid to the right and (f) diagram of structure. (g, h) Show the same information for RT13a respectively. (For interpretation of the references to colour in this figure legend, the reader is referred to the web version of this article.)

#### $n\text{SrTiO}_3 \cdot m\text{TiO}_2$ .

If atoms are removed from this surface, creating surface vacancies, according to integer amounts of either  $\text{SrTiO}_3$  or  $\text{TiO}_2$ , no partially occupied sites exist, there is no overall formal charge for the structure, and a variety of permutations representing possible structures can be generated. Alternatively, experimental data can be used to inform where these vacancies, especially those of the topmost  $\text{TiO}_x$  layers, are most likely to be, as was the case for structures presented here. In cases where the removal of one or more Sr atoms is necessary, the lowest-energy sites for removal, found through DFT simulation, are those with the highest number of neighboring  $\text{TiO}_5$  and  $\text{TiO}_6$  surface units. This is likely due to the fact that removing a Sr atom from these sites does little to impact the bonding environment of the nearby oxygen atoms.

Although both the RT7b and RT13b are rotated with respect to the bulk, this vacancy model extends to unit cells without these rotations. For example, the previously solved  $p3(2 \times 2)a$  structure [48] fits this model and is in fact the smallest possible unit cell for this family. It represents the case of the highest possible  $\text{SrTiO}_3$  vacancy density where the  $p3$  symmetry is maintained. A representation of the  $p3(2 \times 2)a$ , RT7b, and RT13b structures in the framework described above is illustrated in Fig. 5. For the sake of clarity, any removed Sr

atoms are not shown in the symbolic representations of Fig. 5 (e, f). This representation makes clear which sites  $\text{TiO}_5$  or  $\text{TiO}_6$  units occupy. These representations also make the  $\text{TiO}_5$ : $\text{TiO}_6$  ratio easier to gauge at a glance and show how changing the number and placement of vacancies affects this ratio.

This model also provides a framework for understanding defects in reconstructions, particularly those observed in the STM images of the RT13 surfaces shown in Fig. 6(a). These defects appear as breaks in the honeycomb structure of the RT13, leading to the joining of two or more dark areas. If the RT13b structure is examined, some number,  $n$ , of  $\text{TiO}_2$  units (or  $\text{SrTiO}_3$  units) can be removed, as illustrated in Fig. 6 (b, c). In Fig. 6 (b, c) the unit removed is circled in the upper left with the resulting structure after removal shown in the center. While the examples shown maintain  $p3$  symmetry, this is not a necessary condition, and any combination of units can be removed to best capture the experimental STM intensities of a given defect. The Schottky defects illustrated in Fig. 6 (b, c) represent possible structure solutions for defects such as the ones shown in Fig. 6(a).

While this model does not encompass all solved structures on the  $\text{SrTiO}_3(111)$  surface, it can be applied to any reconstruction bearing only  $p3$  symmetry regardless of rotation or size with respect to the bulk

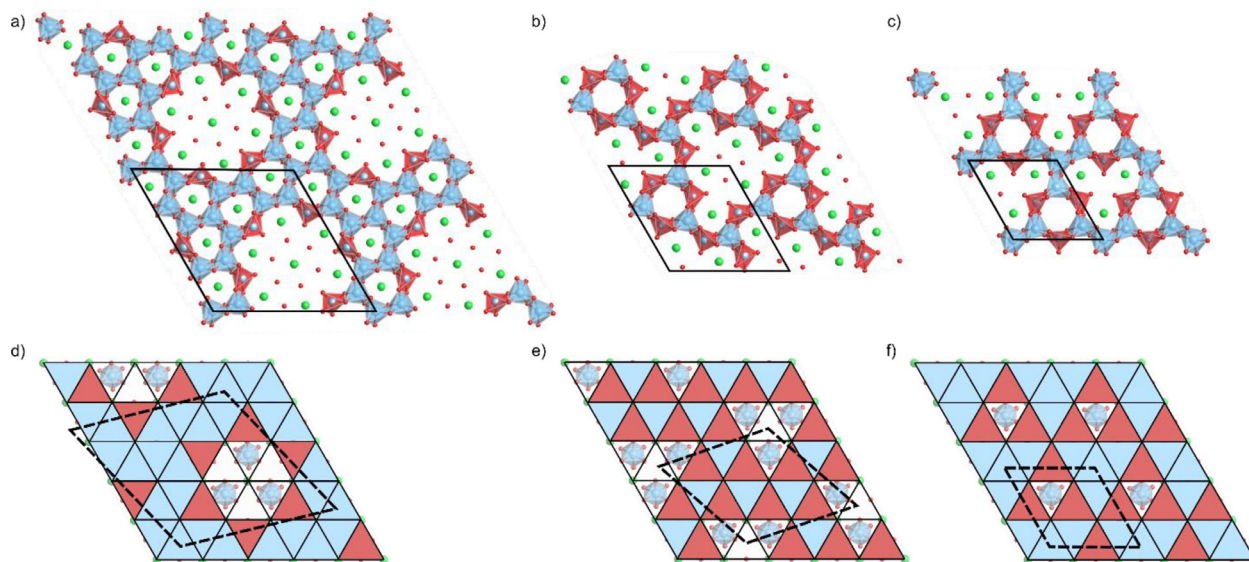


**Fig. 5.** (a) Diagram of RT13b, (b) RT7b, and (c)  $(2 \times 2)a$  where  $\text{TiO}_5$  octahedra are red,  $\text{TiO}_6$  octahedra blue, and Sr atoms are green. (d) Grid imposed on bulk  $\text{SrTiO}_3(111)$  to codify RT13b, (e) RT7b, and (f)  $(2 \times 2)a$ . (For interpretation of the references to colour in this figure legend, the reader is referred to the web version of this article.)

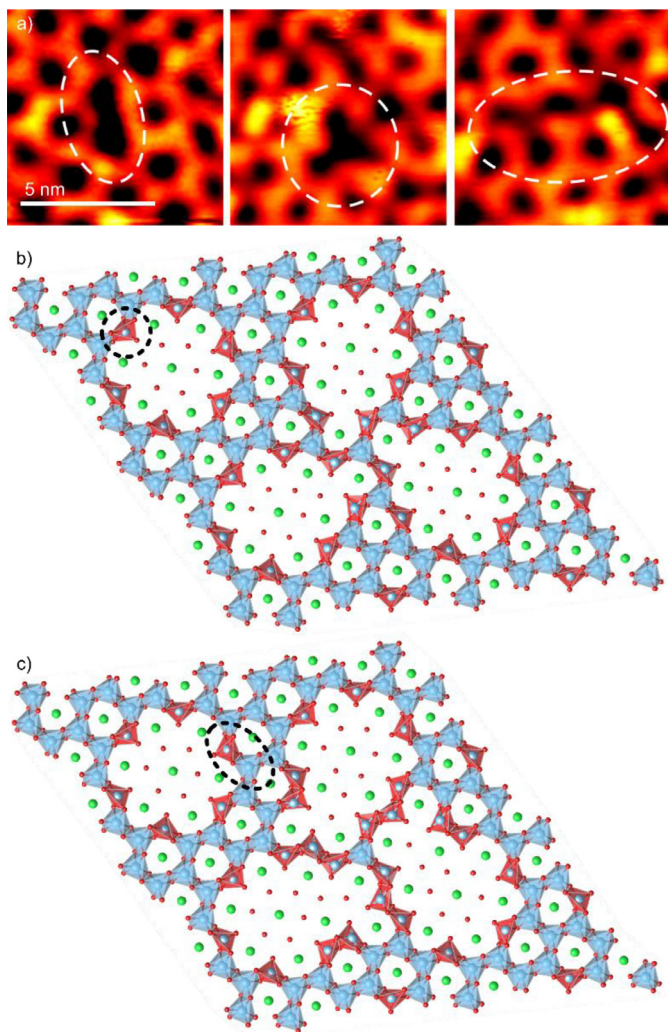


**Fig. 6.** (a) STM image (+2.9 V sample bias, 0.3 nA tunneling current) of defects in RT13. (b, c) Diagrams of RT13b showing possible Schottky defects where TiO<sub>5</sub> octahedra are red, TiO<sub>6</sub> octahedra blue, and Sr atoms are green. (For interpretation of the references to colour in this figure legend, the reader is referred to the web version of this article.)

unit cell. The RT7b and RT13b, along with p3 (2 × 2)a, provide insight into the structure of lower TiO<sub>2</sub>-excess reconstructions where only a single layer of TiO<sub>x</sub> is present. Additionally, they fit in with the other solved Ti double-layer reconstructions on this surface, both structurally and conceptually. The units of this TiO<sub>x</sub> layer are identical to those present in higher-coverage surfaces, like the (3 × 3) and (4 × 4), which also contain TiO<sub>5</sub> and TiO<sub>6</sub> units. However, these single-layer reconstructions require no additional tetrahedral TiO<sub>4</sub>, instead relying on their denser coverage to lower surface energy and provide sufficient electron density for oxygen atoms.

## 5. Conclusions

In summary, the structures of the RT7 and RT13 on the SrTiO<sub>3</sub> (111) surface were identified. The method used considered STM data to produce structural hypotheses that were relaxed via DFT to find low-energy candidates which were compared back to experimental data via STM simulation. The model discussed herein for reconstructions on the SrTiO<sub>3</sub> (111) surface serves as a starting point for generating structural solutions even with sparse data sets, which can be paired with DFT calculations to identify low-energy candidates. Although the hexagonal nature of this surface presents additional complexity, all possible

reconstructions belonging to the described vacancy family of a given unit cell size could be generated via a properly constrained algorithm. Understanding the fundamental units of reconstruction families such as this allows reduction of the computation resources required in identifying structures and provides an opportunity to unify descriptions of reconstructions on a given material surface.

## Acknowledgements

This work used the Extreme Science and Engineering Discovery Environment (XSEDE), which is supported by National Science Foundation grant number ACI-1548562. Specifically, it used the Bridges system, which is supported by NSF award number ACI-1445606, at the Pittsburgh Supercomputing Center (PSC) through allocation DMR160023P [59,60]. T.K.A. and D.D.F. were supported by the U.S. Department of Energy, Office of Science, Office of Basic Energy Sciences, Materials Sciences and Engineering Division.

## Supplementary materials

Supplementary material associated with this article can be found, in the online version, at doi:<https://doi.org/10.1016/j.susc.2018.04.011>.

## References

- [1] Y. Lin, J. Wen, L. Hu, R.M. Kennedy, P.C. Stair, K.R. Poeppelmeier, L.D. Marks, Synthesis-dependent atomic surface structures of oxide nanoparticles, *Phys. Rev. Lett.* 111 (2013) 156101.
- [2] J.G. Mavroides, J.A. Kafalas, D.F. Kolesar, Photoelectrolysis of water in cells with SrTiO<sub>3</sub> anodes, *Appl. Phys. Lett.* 28 (1976) 241–243.
- [3] A. Biswas, P.B. Rossen, C.-H. Yang, W. Siemons, M.-H. Jung, I.K. Yang, R. Ramesh, Y.H. Jeong, Universal Ti-rich termination of atomically flat SrTiO<sub>3</sub> (001), (110), and (111) surfaces, *Appl. Phys. Lett.* 98 (2011) 051904.
- [4] J.H. Lee, G. Luo, I.C. Tung, S.H. Chang, Z. Luo, M. Malshe, M. Gadre, A. Bhattacharya, S.M. Nakhmanson, J.A. Eastman, H. Hong, J. Jellinek, D. Morgan, D.D. Fong, J.W. Freeland, Dynamic layer rearrangement during growth of layered oxide films by molecular beam epitaxy, *Nat. Mater.* 13 (2014) 879–883.
- [5] H.Y. Hwang, Y. Iwasa, M. Kawasaki, B. Keimer, N. Nagaosa, Y. Tokura, Emergent phenomena at oxide interfaces, *Nat. Mater.* 11 (2012) 103–113.
- [6] J. Mannhart, D.G. Schlom, Oxide interfaces- an opportunity for electronics, *Science* 327 (2010) 1607–1611.
- [7] J.M. Rondinelli, S.J. May, J.W. Freeland, Control of octahedral connectivity in perovskite oxide heterostructures: an emerging route to multifunctional materials discovery, *MRS Bull.* 37 (2012) 261–270.
- [8] H. Takagi, H.Y. Hwang, An emergent change of phase for electronics, *Science* 327 (2010) 1601–1602.
- [9] Z. Yang, C. Ko, S. Ramanathan, Oxide electronics utilizing ultrafast metal-insulator transitions, *Annu. Rev. Mater. Res.* 41 (2011) 337–367.
- [10] P. Zubko, S. Gariglio, M. Gabay, P. Ghosez, J.-M. Triscone, Interface physics in complex oxide heterostructures, *Annu. Rev. Condens. Matter Phys.* 2 (2011) 141–165.
- [11] A.N. Chiamonti, Structure and Thermodynamics of Model Catalytic Oxide Surfaces, Northwestern University, Evanston, IL, USA, 2005.
- [12] V.E. Henrich, G. Dresselhaus, H.J. Zeiger, Surface defects and the electronic structure of SrTiO<sub>3</sub> surfaces, *Phys. Rev. B Condens. Matter* 17 (1978) 4908–4921.
- [13] B. Cord, R. Courths, Electronic study of SrTiO<sub>3</sub> (001) surfaces by photoemission, *Surf. Sci.* 162 (1985) 34–38.
- [14] J.E.T. Andersen, P.J. Möller, Impurity-induced 900°C (2 × 2) surface reconstruction of SrTiO<sub>3</sub> (100), *Appl. Phys. Lett.* 56 (1990) 1847–1849.
- [15] T. Matsumoto, H. Tanaka, T. Kawai, S. Kawai, STM-imaging of a SrTiO<sub>3</sub> (100) surface with atomic-scale resolution, *Surf. Sci. Lett.* 278 (1992) L153–L158.
- [16] H. Tanaka, T. Matsumoto, T. Kawai, S. Kawai, Surface structure and electronic property of reduced SrTiO<sub>3</sub> (100) surface observed by scanning tunneling microscopy/spectroscopy, *Jpn. J. Appl. Phys.* 32 (1993) 1405–1409.
- [17] M. Naito, H. Sato, Reflection high-energy electron diffraction study on the SrTiO<sub>3</sub> surface structure, *Physica C* 229 (1994) 1–11.
- [18] Q.D. Jiang, J. Zegenhagen, SrTiO<sub>3</sub> (001) surfaces and growth of ultra-thin GdBa<sub>2</sub>Cu<sub>3</sub>O<sub>7-x</sub> films studied by LEED/AES and UHV-STM, *Surf. Sci.* 338 (1995) L882–L888.
- [19] M. Kawasaki, A. Ohtomo, T. Arakane, K. Takahashi, M. Yoshimoto, H. Koinuma, Atomic control of SrTiO<sub>3</sub> surface for perfect epitaxy of perovskite oxides, *Appl. Surf. Sci.* 107 (1996) 102–106.
- [20] R. Akiyama, T. Matsumoto, H. Tanaka, T. Kawai, Electric field and contact interactions of tip with adenine molecules on SrTiO<sub>3</sub> (100)-√5 × √5 surfaces, *Jpn. J. Appl. Phys.* 36 (1997) 3881–3886.
- [21] J. Zegenhagen, T. Haage, Q.D. Jiang, Microscopic structure and structuring of perovskite surfaces and interfaces: SrTiO<sub>3</sub>, RBa<sub>2</sub>Cu<sub>3</sub>O<sub>7-δ</sub>, *Appl. Phys. A* 67 (1998) 711–722.

- [22] P.J. Møller, S.A. Komolov, E.F. Lazneva, Selective growth of a MgO (100)-c(2 × 2) superstructure on a SrTiO<sub>3</sub> (100)-(2 × 2) substrate, *Surf. Sci.* 425 (1999) 15–21.
- [23] G. Charlton, S. Brennan, C.A. Muryn, R. McGrath, D. Norman, T.S. Turner, G. Thornton, Surface relaxation of SrTiO<sub>3</sub> (001), *Surf. Sci.* 457 (2000) L376–L380.
- [24] M.S.M. González, M.H. Aguirre, E. Morán, M.Á. Alario-Franco, V. Perez-Dieste, J. Avila, M.C. Asensio, In situ reduction of (100) SrTiO<sub>3</sub>, *Solid State Sci.* 2 (2000) 519–524.
- [25] T. Kubo, H. Nozoye, Surface structure of SrTiO<sub>3</sub> (100)-(√5 × √5)R26.6°, *Phys. Rev. Lett.* 86 (2001) 1801–1804.
- [26] P.A.W. van der Heide, Q.D. Jiang, Y.S. Kim, J.W. Rabalais, X-ray photoelectron spectroscopic and ion scattering study of the SrTiO<sub>3</sub> (001) surface, *Surf. Sci.* 473 (2001) 59–70.
- [27] M.R. Castell, Scanning tunneling microscopy of reconstructions on the SrTiO<sub>3</sub> (001) surface, *Surf. Sci.* 505 (2002) 1–13.
- [28] M.R. Castell, Nanostructures on the SrTiO<sub>3</sub> (001) surface studied by STM, *Surf. Sci.* 516 (2002) 33–42.
- [29] N. Erdman, K.R. Poepplmeier, M. Asta, O. Warschkow, D.E. Ellis, L.D. Marks, The structure and chemistry of the TiO<sub>2</sub>-rich surface of SrTiO<sub>3</sub> (001), *Nature* 419 (2002) 55–58.
- [30] N. Erdman, O. Warschkow, M. Asta, K.R. Poepplmeier, D.E. Ellis, L.D. Marks, Surface structures of SrTiO<sub>3</sub> (001): A TiO<sub>2</sub>-rich reconstruction with a c(4 × 2) unit cell, *J. Am. Chem. Soc.* 125 (2003) 10050–10056.
- [31] T. Kubo, H. Nozoye, Surface structure of SrTiO<sub>3</sub> (100), *Surf. Sci.* 542 (2003) 177–191.
- [32] C.H. Lanier, A. van de Walle, N. Erdman, E. Landree, O. Warschkow, A. Kazimirov, K.R. Poepplmeier, J. Zegenhagen, M. Asta, L.D. Marks, Atomic-scale structure of the SrTiO<sub>3</sub> (001)-c(6 × 2) reconstruction: experiments and first-principles calculations, *Phys. Rev. B Condens. Matter* 76 (2007) 045421.
- [33] Y. Lin, A.E. Becerra-Toledo, F. Silly, K.R. Poepplmeier, M.R. Castell, L.D. Marks, The (2 × 2) reconstructions on the SrTiO<sub>3</sub> (001) surface: a combined scanning tunneling microscopy and density functional theory study, *Surf. Sci.* 605 (2011) L51–L55.
- [34] O. Warschkow, M. Asta, N. Erdman, K.R. Poepplmeier, D.E. Ellis, L.D. Marks, TiO<sub>2</sub>-rich reconstructions of SrTiO<sub>3</sub> (001): a theoretical study of structural patterns, *Surf. Sci.* 573 (2004) 446–456.
- [35] D.M. Kienzle, A.E. Becerra-Toledo, L.D. Marks, Vacant-site octahedral tilings on SrTiO<sub>3</sub> (001), the (√13 × √13)R33.7° surface, and related structures, *Phys. Rev. Lett.* 106 (2011) 176102.
- [36] H. Bando, Y. Aiura, Y. Haruyama, T. Shimizu, Y. Nishihara, Structure and electronic states on reduced SrTiO<sub>3</sub> (110) surface observed by scanning tunneling microscopy and spectroscopy, *J. Vac. Sci. Technol. B* 13 (1995) 1150–1154.
- [37] J. Brunen, J. Zegenhagen, Investigation of the SrTiO<sub>3</sub> (110) surface by means of LEED, scanning tunneling microscopy and Auger spectroscopy, *Surf. Sci.* 389 (1997) 349–365.
- [38] Y. Mukunoki, N. Nakagawa, T. Susaki, H.Y. Hwang, Atomically flat (110) SrTiO<sub>3</sub> and heteroepitaxy, *Appl. Phys. Lett.* 86 (2005) 171908.
- [39] B.C. Russell, M.R. Castell, Reconstructions on the polar SrTiO<sub>3</sub> (110) surface: analysis using STM, LEED, and AES, *Phys. Rev. B Condens. Matter* 77 (2008) 245414.
- [40] J.A. Enterkin, A.K. Subramanian, B.C. Russell, M.R. Castell, K.R. Poepplmeier, L.D. Marks, A homologous series of structures on the surface of SrTiO<sub>3</sub> (110), *Nat. Mater.* 9 (2010) 245–248.
- [41] F. Li, Z. Wang, S. Meng, Y. Sun, J. Yang, Q. Guo, J. Guo, Reversible transition between thermodynamically stable phases with low density of oxygen vacancies on the SrTiO<sub>3</sub> (110) surface, *Phys. Rev. Lett.* 107 (2011) 036103.
- [42] Z. Wang, A. Loon, A. Subramanian, S. Gerhold, E. McDermott, J.A. Enterkin, M. Hieckel, B.C. Russell, R.J. Green, A. Moewes, J. Guo, P. Blaha, M.R. Castell, U. Diebold, L.D. Marks, Transition from reconstruction toward thin film on the (110) surface of strontium titanate, *Nano Lett.* 16 (2016) 2407.
- [43] A. Gömann, K. Gömann, M. Frerichs, V. Kempter, G. Borchardt, W. Maus-Friedrichs, Electronic structure and topography of annealed SrTiO<sub>3</sub> (111) surfaces studied with MIES and STM, *Appl. Surf. Sci.* 252 (2005) 196–199.
- [44] Y. Haruyama, Y. Aiura, H. Bando, Y. Nishihara, H. Kato, Annealing temperature dependence on the electronic structure of the reduced SrTiO<sub>3</sub> (111) surface, *J. Electron. Spectrosc. Relat. Phenom.* 88 (1998) 695–699.
- [45] S. Sekiguchi, M. Fujimoto, M. Nomura, S.-B. Cho, J. Tanaka, T. Nishihara, M.-G. Kang, H.-H. Park, Atomic force microscopic observation of SrTiO<sub>3</sub> polar surface, *Solid State Ionics* 108 (1998) 73–79.
- [46] A.N. Chiamonti, C.H. Lanier, L.D. Marks, P.C. Stair, Time, temperature, and oxygen partial pressure-dependent surface reconstructions on SrTiO<sub>3</sub> (111): a systematic study of oxygen-rich conditions, *Surf. Sci.* 602 (2008) 3018–3025.
- [47] B.C. Russell, M.R. Castell, Surface of sputtered and annealed polar SrTiO<sub>3</sub> (111): TiO<sub>x</sub>-Rich (n × n) reconstructions, *J. Phys. Chem. C* 112 (2008) 6538–6545.
- [48] L.D. Marks, A.N. Chiamonti, S.U. Rahman, M.R. Castell, Transition from order to configurational disorder for surface reconstructions on SrTiO<sub>3</sub> (111), *Phys. Rev. Lett.* 114 (2015) 226101.
- [49] B.C. Russell, M.R. Castell, (√13 × √13)R13.9° and (√7 × √7)R19.1° reconstructions of the polar SrTiO<sub>3</sub> (111) surface, *Phys. Rev. B Condens. Matter* 75 (2007) 155433.
- [50] P. Blaha, K. Schwarz, G.K.H. Madsen, D. Kvasnicka, J. Luitz, WIEN2k, an Augmented Plane Wave + Local Orbitals Program for Calculating Crystal Properties, Universität Wien, Austria, 2010.
- [51] J.P. Perdew, K. Burke, M. Ernzerhof, Generalized gradient approximation made simple, *Phys. Rev. Lett.* 77 (1996) 3865–3868.
- [52] V.N. Staroverov, G.E. Scuseria, J. Tao, J.P. Perdew, Comparative assessment of a new nonempirical density functional: molecules and hydrogen-bonded complexes, *J. Chem. Phys.* 119 (2003) 12129–12137.
- [53] L.D. Marks, Fixed-point optimization of atoms and density in DFT, *J. Chem. Theor. Comput.* 9 (2013) 2786–2800.
- [54] J. Tersoff, D.R. Hamann, Theory of the scanning tunneling microscope, *Phys. Rev. B Condens. Matter* 31 (1985) 805–813.
- [55] A.E. Becerra-Toledo, M.S.J. Marshall, M.R. Castell, L.D. Marks, c(4 × 2) and related structural units on the SrTiO<sub>3</sub> (001) surface: scanning tunneling microscopy, density functional theory, and atomic structure, *J. Chem. Phys.* 136 (2012) 214701.
- [56] L. Jones, H. Yang, T.J. Pennycook, M.S.J. Marshall, S. Van Aert, N.D. Browning, M.R. Castell, P.D. Nellist, Smart align—a new tool for robust non-rigid registration of scanning microscope data, *Adv. Struct. Chem. Imaging* 1 (2015) 8.
- [57] J.A. Enterkin, A.E. Becerra-Toledo, K.R. Poepplmeier, L.D. Marks, A chemical approach to understanding oxide surfaces, *Surf. Sci.* 606 (2012) 344–355.
- [58] L.D. Marks, A.N. Chiamonti, F. Tran, P. Blaha, The small unit cell reconstructions of SrTiO<sub>3</sub> (111), *Surf. Sci.* 603 (2009) 2179–2187.
- [59] N. Nystrom, M. Levine, R. Roskies, J. Scott, Bridges: a uniquely flexible HPC resource for new communities and data analytics, in, 2015, pp. 1–8.
- [60] J. Towns, T. Cockerill, M. Dahan, I. Foster, K. Gathier, A. Grimshaw, V. Hazlewood, S. Lathrop, D. Lifka, G.D. Peterson, R. Roskies, J.R. Scott, N. Wilkins-Diehr, XSEDE: accelerating scientific discovery, *Comput. Sci. Eng.* 16 (2014) 62–74.